Journal of Applied Polymer Science

Study on the Structure, Morphology, and Properties of End-Functionalized Star-Shaped Solution-Polymerized Styrene-Butadiene Rubber

Yu Bai,[1] Suhe Zhao,[1,2] Yuanyuan Tong,[1] Xingying Zhang,[1,2] Xiao Liu,[1] Miao Tian[1]

[1]Key Laboratory of Beijing City on Preparation and Processing of Novel Polymer Materials, College of Material Science and Engineering, Beijing University of Chemical Technology, Beijing 100029, People's Republic of China

[2]Key Laboratory of Carbon Fiber and Functional Polymers, Ministry of Education, College of Material Science and Engineering, Beijing University of Chemical Technology, Beijing 100029, People's Republic of China

Correspondence to: S. Zhao (E-mail: Zhaosh@mail.buct.edu.cn)

ABSTRACT: Three kinds of star-shaped solution-polymerized styrene–butadiene rubber (S-SSBR) were synthesized by living anionic polymerization using a self-made multifunctional organic lithium initiator. One was S-SSBR with 100% coupling degree. Others were the functionalized S-SSBR which had macromolecular chain-free ends terminated directly (ES-SSBR-1), and macromolecular chain terminated after dissociation in the polymerization solution (ES-SSBR-2) by 3-chloropropyl trimethoxy siloxane. The molecular structure parameters of three kinds of SSBR were determined and the end-functionalized efficiency was calculated. The rheological properties, mechanical properties, and dynamic mechanical properties of ES-SSBR and S-SSBR composites filled with silica (SiO_2)–carbon black (CB) were investigated. The morphology was observed by transmission electron microscopy and high-resolution transmission electron microscopy, and the dispersion of the two kinds of filler in the composites was distinguished by X-ray energy spectrometry. The results showed that the mixing speed of hydrophilic SiO_2 powder in the ES-SSBR was higher than that in the S-SSBR. SiO_2-CB/ES-SSBR composites presented excellent mechanical properties, high wet-skid resistance, and low rolling resistance. Two kinds of nanofiller in the ES-SSBR exhibited outstanding doping nanometer dispersion and good distribution, which indicated that after being coupled and end-functionalized, the two free ends of the macromolecular chains formed chemical bonding with the surface chemical groups of CB and SiO_2, respectively. Accordingly, ES-SSBR was a remarkable energy-saving elastomer. © 2012 Wiley Periodicals, Inc. J. Appl. Polym. Sci. 000: 000–000, 2012

KEYWORDS: addition polymerization; elastomers; nanocomposites; silicas

Received 1 June 2011; accepted 4 July 2012; published online
DOI: 10.1002/app.38430

INTRODUCTION

Recently, with the rapid development of the automotive industry and the increasing shortage of oil resources, energy conservation and environmental protection have been the focus of vehicle manufacturers. The reduction of fuel consumption of vehicle is the most direct and effective measure to protect the environment. Survey shows that the energy used to overcome rolling resistance accounts for 14.4% of the total energy consumption of automobiles.[1] Besides, from the distribution of energy consumption of the tire, the rolling losses of tread make up about 49% of energy consumption.[2] Therefore, the reduction of energy consumption of tread rubber can save energy and reduce the carbon emissions of automobiles.

As is well known to us, the rolling resistance of tire tread is mainly caused by hysteresis loss, and decreasing or inactivating the free ends of molecular chains in the three-dimensional crosslinked network of vulcanized rubber is the most effective way to reduce hysteresis loss. According to this idea, solution-polymerized styrene–butadiene rubber (SSBR) coupled partly with $SnCl_4$ is a typical product commercialized with improved energy conservation and high wet-skid resistance. As parts of the macromolecular chain terminals are coupled by Sn, the internal friction caused by the random thermal motion of the free chain ends is reduced. Furthermore, the Sn—C bond is weaker than the C—C bond and is easy to break during mixing. The free radicals produced can react with the free electrons on the surface of carbon black (CB). The reaction strengthens the interaction of rubber and CB and at the same time improves the dispersion of CB in the SSBR. Zhao et al.[3] have shown that with increasing coupling degree of SSBR the internal friction

Applied Polymer SCIENCE

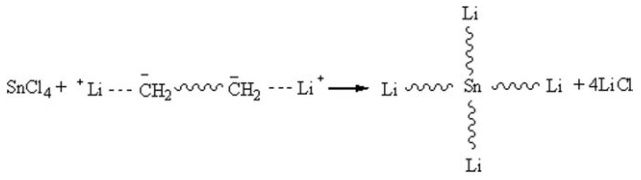

Figure 1. The reaction formula for multifunctional lithium initiator.

losses are reduced. SSBR coupled partly with $SnCl_4$ has been produced in the Netherlands, Japan, and the United States, and fully used in high-speed tires. Recently, Zhang et al.[4,5] have invented a multifunctional organic lithium initiator by the use of which a fully coupled SSBR (C-SSBR) is synthesized in one step. As half of the macromolecular chain ends of C-SSBR are bound, its molecular structure parameters and array distribution of monomer units are reasonable. This kind of SSBR shows lower rolling resistance, higher wet-skid resistance, and higher wear resistance than partly couple SSBR.[3]

Introducing functional groups that can either react with the nanofiller or inactivate the free chain ends is another effective way to lower internal friction losses. Investigators at JSR Bridgestone[6] have attached the siloxane group to the end of SSBR macromolecular chains and obtained a remarkable improvement in energy saving. Li et al.[7,8] have used 3-chloropropyl trimethoxy siloxane (CPTMO) which can react with SiO_2 as an end-capper, to modify linear SSBR, resulting in significant improvements in mechanical and dynamic mechanical properties, and filler dispersion of the composites. Wang et al.[9] have modified linear SSBR with *tert*-butylchlorodiphenylsilane (large-volume functional group), resulting in the linking of double-benzene ring groups to the two ends of the SSBR molecular chain. These ring groups can restrain the movement of the molecular chain ends, and at the same time the large-volume functional groups showed a good affinity to the CB. Thus, the CB can be well distributed in the SSBR matrix, and the Payne effect of the composites reduced. This kind of SSBR showed excellent overall properties and low internal friction losses.

Based on the idea of modifying molecular chain ends and the results of our previous investigations,[3–10] we tried to prepare a *di*-functional energy-saving SSBR, whose molecular chain is coupled by tin at one end and modified by a functional group at the other. The two ends of the modified molecular chain can react with active groups on the surface of CB and SiO_2, respectively. The purpose of this study is to prepare a new energy-saving elastomer without free chain ends.

In this study, a star-shaped (100% coupling degree) SSBR and two ES-SSBRs (star-shaped SSBR end-capped by CPTMO) were prepared by anionic polymerization. The molecular structure parameters of the SSBR and ES-SSBRs were determined and the end-functionalized efficiency of the ES-SSBRs was calculated. The rheological properties, mechanical properties, and dynamic mechanical properties of the ES-SSBR and S-SSBR composites filled with SiO_2–CB diphasic filler were investigated. The morphology was observed by transmission electron microscopy (TEM). The experimental results are expected to provide theoretical and practical bases for the structure design, implementation, and performance evaluation of energy-saving rubbers.

EXPERIMENTAL

Materials

Styrene (St) (analysis grade) was produced by Beijing Chemical Reagents (Beijing, China). Butadiene (polymerization grade) was provided by Beijing Yanshan Petrochemical (Beijing, China). Tetrahydrofuran (THF) (analysis grade) was supplied by Beijing Chemical Works (Beijing, China). Multifunctional lithium initiator[4] and dissociation agent were self-prepared in the laboratory. CPTMO (98% purity, industrial grade) was obtained from Qufu Wanda Chemical (Shandong, China). CB (N234) was purchased from Tianjin Haitun Carbon Black (Tianjin, China). The precipitated silica (Tixosil 383) was produced by Qingdao Rhodia (Shandong, China). All other reagents, such as zinc oxide, stearic acid, and sulfur, were of commercial grades.

Polybutadiene with double lithium active short chain prepared by Naphthalene lithium reaction with a fixed amount of butadiene reacted with stannic chloride, and the result was multifunctional lithium initiator. The reaction formula is shown in Figure 1.

The S-SSBR and two ES-SSBRs were synthesized in our laboratory. ES-SSBR is S-SSBR end-capped by CPTMO. The reaction mechanism of ES-SSBR is shown in Figure 2, and the structural parameters of these SSBRs are listed in Table I.

Formulation for Rubber Composites

Composites Formulation is given in Table II.

Specimen Preparation

Preparation of SSBR Samples. The purified cyclohexane 580 g, butadiene 75 g, styrene 25 g, THF 4.5 g, and multifunctional lithium initiator 0.5 g were added into a 2-L stainless reactor, and the polymerization lasted 4 h at 50°C, and was terminated by the methanol to obtain the SSBR polymerization solution.

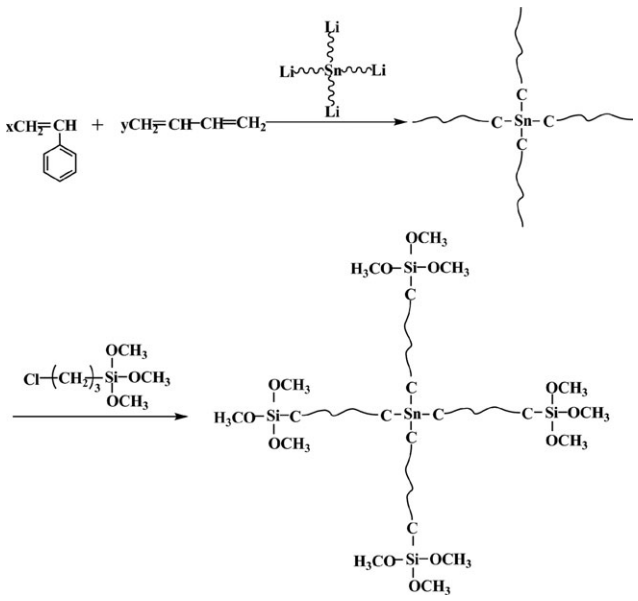

Figure 2. Reaction mechanism of ES-SSBR.

Table I. Structural Parameters of S-SSBR and ES-SSBRs

Compound no.	S-SSBR	ES-SSBR-1	ES-SSBR-2
Mn (g/mol)	197,442	193,529	163,437
Mw (g/mol)	348,545	336,592	288,785
MWD	1.77	1.70	1.77
St[a] (%)	26.0	26.1	24.6
Bv[b] (%)	48.8	41.1	46.1
Atacticity (%)	100	100	100
End-function efficiency (%)	0	8.62	28.5

[a]Styrene content.
[b]Content of vinyl.

Before the polyreaction was terminated, CPTMO of 0.25 g was added into the polymerization solution and allowed to react for 1 h at 65°C to obtain the ES-SSBR-1 polymerization solution. Before adding 0.38 g CPTMO, 0.12 g $CH(CH_3)_2OLi$ (dissociation agent) was added into the polymerization solution to decrease the solution viscosity, and the ES-SSBR-2 polymerization solution was obtained in the same reaction time as the ES-SSBR-1 polymerization solution. Each of the three kinds of polymerization solutions was purified by precipitation with technical alcohol and dried in a vacuum oven. The residue was dissolved repeatedly in cyclohexane, and any unreacted CPTMO and dissociation agent were extracted from the polymer by using technical alcohol. At last, the three polymers S-SSBR, ES-SSBR-1, and ES-SSBR-2 were obtained after being dried to constant weight in the vacuum oven.

Preparation of the Vulcanizates. Silica was mixed into the rubber by a Haake PolyLab torque rheometer equipped with a Rheomix 610p mixing chamber and roller rotors (Thermo Electron, USA) at a temperature of 50°C and a rotating speed of 10 r/min for 30 min. The mixing curves are shown in Figure 3. Reaction blending was done by the same equipment at a temperature of 90°C for 18 min. The remainder of the silica, CB, and other additives was added to the rubber on a 6-in two-roll mill (Shanghai Rubber Machinery Works No. 1, Shanghai, China). The vulcanizate samples were prepared by a plate vulcanization machine (Shanghai Rubber Machinery Works, Shanghai, China) under the curing condition of 150°C × t_{90} (optimum curing time). The SiO_2–CB-filled S-SSBR, ES-SSBR-1, and ES-SSBR-2 composites were marked as A1, A2, and A3, respectively.

Characterization

The number-average molecular weight (Mn), weight-average molecular weight (Mw), and polydispersity index (Mw/Mn) of the three SSBRs were measured by using a Waters 150-C gel permeation chromatograph (Waters, USA) with three Waters Styragel columns (pore size 10^2, 10^3, and 10^4 Å) in series. The columns were calibrated by narrow-distribution polystyrene standards with molecular weights ranging from 2.2×10^3 to 5.15×10^5 g/mol. THF was used as the eluent at a flow rate of 1.0 mL/min at 40°C.

The microstructures of the three SSBRs were confirmed on an AV600 spectrometer (Bruker, Germany) at 600 MHz in $CDCl_3$ and analyzed at room temperature (25°C). Chemical shifts were reported in parts per million (ppm), referenced to tetramethylsilane as internal standard, and calculated by using the residual isotopic impurities of the deuterated solvents.

Rheological properties were determined by an Instron 3211 Capillary Rheometer (Instron, United Kingdom). The testing temperature was 100°C, and the sample was preheated for 10 min before each measurement. The length to diameter ratio of the capillary was 16 : 1, and the plunger speeds were 0.06, 0.2, 0.6, 2.0, 6.0, and 20.0 cm/min. The shear stress was not corrected for entrance effects in the determination of viscosity.

Bound rubber content was determined as follows: About 2 g of rubber composite was cut into small pieces and placed in a package made of copper wire mesh with an average pore diameter of 74 μm. The package was immersed in toluene for 3 days and acetone for 1 day, followed by drying to constant weight at 60°C in a vacuum oven. The toluene was changed every 24 h. The weights of the sample before and after the extraction were measured, and the bound rubber content was calculated according to the following equation:

$$W(\%) = \frac{(W_3 - W_2)}{W_1} \times 100\%$$

where W is the bound rubber content, W_3 is the weight of the rubber after soaking, and W_2 and W_1 are the weights of filler and rubber, respectively, in the composite before soaking.

The tensile strength and tear strength were measured according to Chinese Standards GB/T528-1998 and GB/T529-1999 by the use of a CMT4104 Electrical Tensile Tester (Shenzhen SANS Test Machine, China) at 25 ± 2°C and a stretching rate of 500 mm/min. Shore A hardness of the vulcanizates was measured according to Chinese Standard GB/T531-1999 by the use of a rubber hardness apparatus (4th Chemical Industry Machine Factory, Shanghai, China).

Table II. Composites Formulation

Ingredients	Loading (phr)[a]
SSBR	100.0
Silica	20.0
N234	30.0
Zinc oxide	4.0
Stearic acid	1.0
Polymerized 2,2,4-trimethyl-1, 2-dihydroquinoline	1.5
Dibenzothiazole disulfide	1.2,
Diphenylguanidine	0.6
Triethanolamine	1.0
Aromatic oil	5.0
Sulfur	1.8

[a]phr: parts-per-hundred rubber.

Applied Polymer SCIENCE

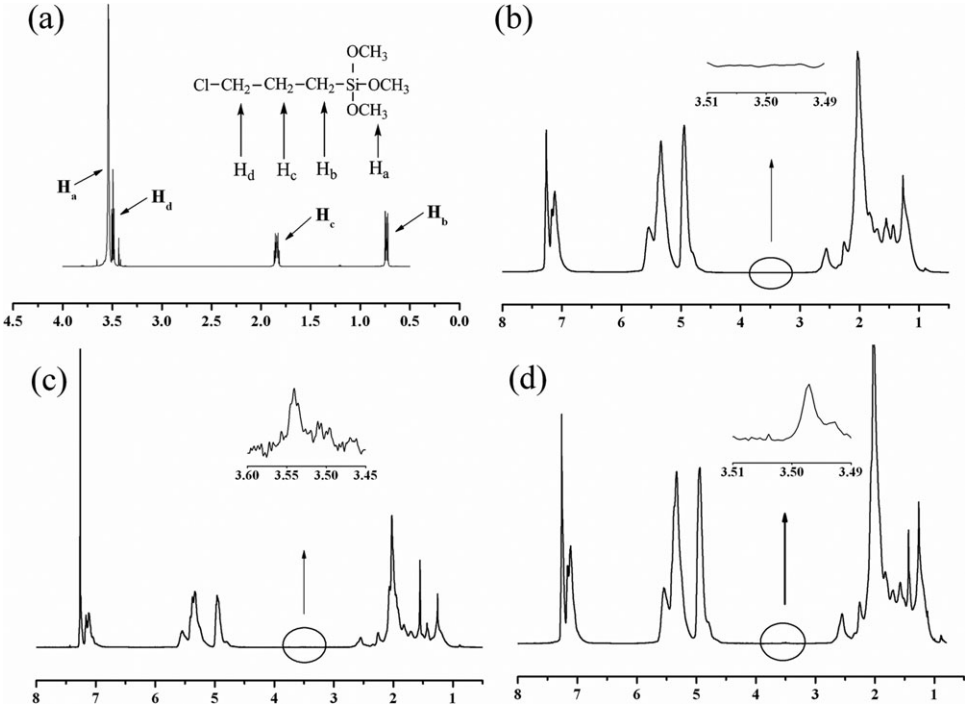

Figure 3. ^{1}H-NMR spectra of (a) CPTMO, (b) S-SBR, (c) ES-SSBR-1, and (d) ES-SSBR-2.

The dynamic compression was determined by a YS-25 Compression Heat Built-Up Tester (Shanghai Rubber Machinery Works, China). Each dynamic compression measurement lasted 25 min at 55°C with a load of 1.01 MPa, a compression stroke of 4.45 mm, and a compression frequency of 30 Hz.

The dynamic mechanical property of the vulcanizates (strain sweep) was measured on a RPA2000 Rubber Process Analyzer (Alpha Technologies, USA). The test temperature was 60°C, the strain was varied from 0.28 to 100%, and the frequency was 1 Hz.

The dynamic mechanical property (temperature sweep) was determined by a VA3000 Dynamic Mechanical Thermal Analyzer (01dB-Metravib, France) in a rectangular tension mode. The testing temperature was from −100 to 100°C, the speed of temperature rise was 3°C/min, the frequency was 10 Hz, and the strain amplitude was 0.1%.

The morphological structure was observed by a Hitachi-800-1 Transmission Electron Microscopy and JEM-3010 High-Resolution Transmission Electron Microscopy (Hitachi, Japan). The acceleration voltages were 200 and 300 KV. The thin sections were cut by a microtome at −100°C and collected on copper grids.

The elements and their distributions in the samples were analyzed by a Genesis-60 X-ray energy spectrometer (EDAX, USA).

RESULTS AND DISCUSSION

Chemical Structure and End-Functionalized Efficiency of ES-SSBR

The ^{1}H NMR spectra of SSBR and ES-SSBR are shown in Figure 3, and the assignment[9] of standard ^{1}H NMR bands is summarized in Table III.

The spectra shown in Figure 3(b–d) all exhibit no resonance peak of block styrene between 6.20 and 6.85 ppm, indicating that the styrene in the molecular chains of all the SSBR samples is random distribution. The peak at 3.54 ppm seen in the spectra in Figure 3(c, d) represents the protons (H) in the $Si(OCH_3)_3$ of CPTMO. This peak cannot be observed in the spectrum in Figure 3(b), indicating that the siloxane groups have been successfully grafted to the ends of the macromolecular chains of ES-SSBR.

In the ^{1}H NMR spectra, the peak area of the five protons (H) derived from the benzene ring in the polymer and that of the nine protons (H) in —Si— $(OCH_3)_3$ can be calculated and are named as $S_{\text{Benzene-H}}$ and $S_{\text{CPTMO-H}}$, respectively. Thus, the

Table III. Assignment of Standard ^{1}H NMR Bands for S-SSBR and ES-SSBR

Chemical shift (ppm)	Structure
7.23, 7.13	Pronton (H) in benzene of random styrene
6.20–6.85	Pronton (H) in benzene (meta and para positions) of block styrene
5.50–5.60	Pronton (H) in =CH— of 1,2-butadiene structural unit
5.10–5.50	Pronton (H) in —CH= of 1,4-butadiene structural unit
4.72–5.10	Pronton (H) in $=CH_2$ of 1,2-butadiene structural unit
3.40–3.60	Pronton (H) in —Si—$(OCH_3)_3$

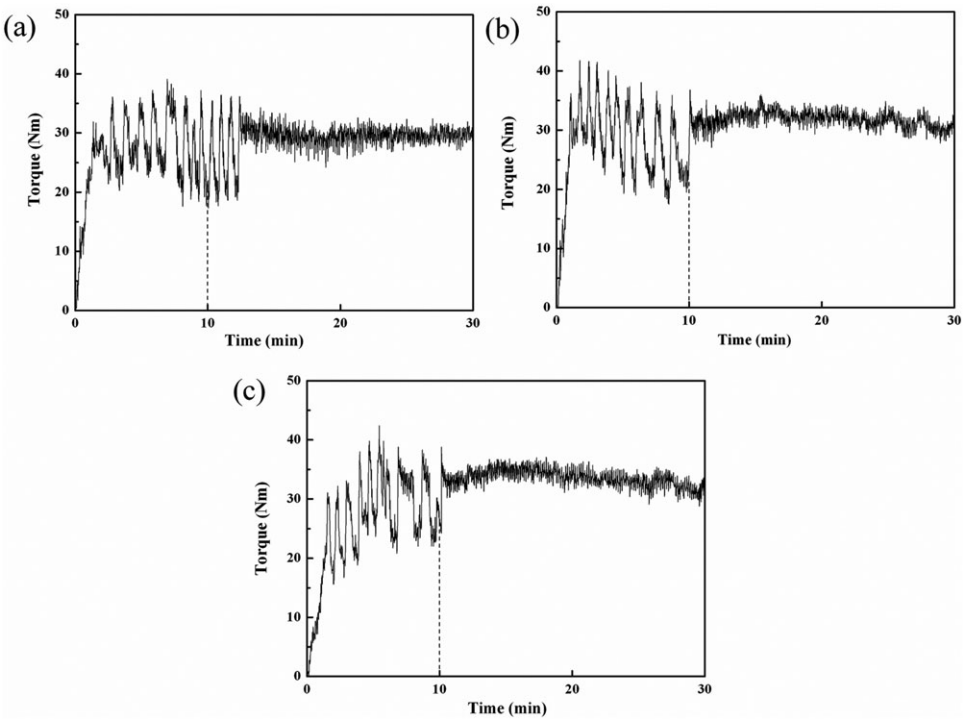

Figure 4. Torque vs. time curves of mixing silica powder with S-SSBR (a), ES-SSBR-1 (b), and ES-SSBR-2 (c) in Haake internal mixer.

end-functionalized efficiency (E) of ES-SSBR can be calculated according to the following formulas:

$$\frac{S_{\text{Benzene-H}}}{S_{\text{CPTMO-H}}} = \frac{\frac{W_m}{(N_1V_1-4N_2V_2)} \times \frac{\text{St\%}}{M_{\text{Benzene}}} \times 5}{1 \times 9 \times E}$$

$$E = \frac{1}{187.2} \times \frac{S_{\text{CPTMO-H}} \times \text{St\%} \times W_m}{S_{\text{Benzene-H}} \times (N_1V_1 - 4N_2V_2)}$$

W_m stands for the mass of monomer. N_1 and N_2 represent the molar concentrations of naphthalene lithium and stannic chloride ($SnCl_4$), respectively, used for preparing the multifunctional lithium initiator. V_1 and V_2 stand for the volumes of naphthalene lithium and $SnCl_4$ solution, respectively. $(N_1V_1 - 4N_2V_2)$ is the mole number of active species in the polymer. St% represents the styrene content. M_{Styrene} is the molecular weight of styrene. The end-functionalized efficiency, as calculated by the above formulas, is listed in Table I.

Processability of Three Kinds of SSBR

Tracing of End-Condensation Reaction. Nanosilica powder was blended with each of S-SSBR, ES-SSBR-1, and ES-SSBR-2 in a Haake PolyLab torque rheometer at the temperature of 50°C, and the torque–time curves of different samples are shown in Figure 4.

As shown in Figure 4, the torque fluctuates remarkably in the first 10 min, which is the time of adding silica powder to the rubber matrix, and the torques of the two ES-SSBRs fluctuate to a greater extent than that of the S-SSBR. Additionally, the torque values of the ES-SSBR samples reach steady state right after silica powder is added. However, the torque of the S-SSBR sample takes another 3.5 min to reach steady state, meaning that the mixing time of SiO_2 powder in ES-SSBR is shorter than that in S-SSBR (26% shorter). The steady-state torque values for S-SSBR, ES-SSBR-1, and ES-SSBR-2 are 30, 33, and 35 Nm, respectively. These results demonstrate that excellent filler

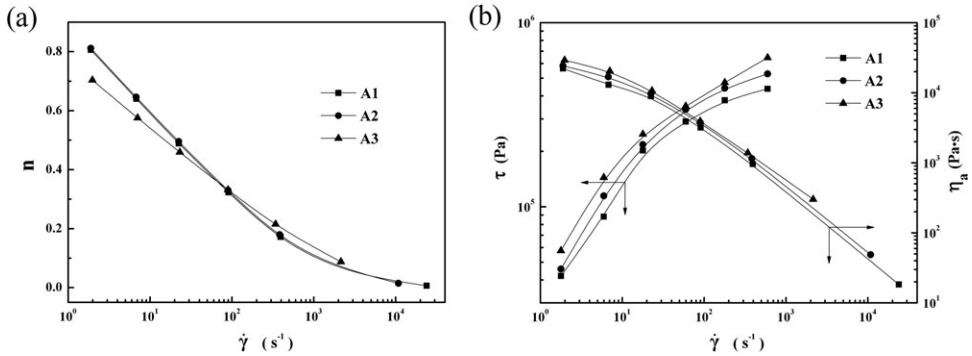

Figure 5. Flow curves of SiO_2–CB/S-SSBR and SiO_2–CB/ES-SSBR composites: (a) n vs. $\dot{\gamma}$ and (b) τ vs. $\dot{\gamma}$ and η_a vs. $\dot{\gamma}$.

Table IV. Bound Rubber Contents of SiO_2–CB/S-SSBR and SiO_2–CB/ES-SSBR Composites

Sample no.	A1	A2	A3
Bound rubber content (%)	12.6	30.29	42.61

dispersion and strong filler–polymer interaction can be achieved by condensation reaction between the functionalized groups at the ends of the macromolecule and the silica powder. The steady-state torque value of ES-SSBR-2 is higher than that of ES-SSBR-1 because ES-SSBR-2 has a higher end-functionalized efficiency than ES-SSBR-1.

Rheological Properties. The flow curves of SiO_2–CB/S-SSBR and the two SiO_2–CB/ES-SSBR composites are shown in Figure 5.

As is clearly shown in Figure 5, the non-Newtonian index (n) and apparent viscosity (η_a) of the three composites both decrease with increasing shear rate (γ), indicating that all three composites are shear-thinning non-Newtonian fluids. What is more, A1 has the lowest shear stress (τ) and apparent viscosity (η_a) of the three composites. In other words, the flowability of A2 and A3 is worse than that of A1. It is the condensation reaction between the functional ends of molecular chains and the silica powder that contributes to the high viscosity and long relaxation during flow.

Filler–Matrix Interaction and the Properties of Composites

Bound Rubber Content. The bound rubber contents of the three compounds are listed in Table IV.

Table IV summarizes that A2 and A3 have higher bound rubber contents than A1 because the chemical bonding between the filler and the polymer is stronger in A2 and A3 than in A1. A3 has the highest bound rubber content because its end-functionalized efficiency is the highest.

Mechanical Properties. The mechanical properties of the three composites are summarized in Table V.

Table V summarizes that the order of Shore A hardness for the three composites is as follows: A1 > A2 > A3, whereas that of

Table V. Mechanical Properties of SiO_2–CB/S-SSBR and SiO_2–CB/ES-SSBR composites

Mechanical parameter	A1	A2	A3
Shore A hardness	69	66	65
Modulus at 100% elongation (MPa)	1.8	2.0	1.8
Modulus at 300% elongation (MPa)	6.2	8.6	8.8
Tensile strength (MPa)	19.6	19.5	21.2
Elongation at break (%)	573	492	496
Permanent set (%)	28	16	16
Tear strength (kN/m)	34.7	38.2	34.7
Compression heat build-up (°C)	15.0	12.1	12.7
Compression permanent set (%)	5.5	2.8	3.2

modulus at 300% elongation is reversed, demonstrating better filler dispersion as well as stronger interaction between the nanofiller and the rubber matrix in samples A2 and A3 than in sample A1. What is more, the elongation at break, permanent set, and compression heat build-up of samples A2 and A3 are significantly lower than those of sample A1. On the other hand, the tensile strength and tear strength of samples A2 and A3 are slightly higher than those of sample A1. These results show that the filler–polymer interaction is strengthened and the random thermal motion of the chain terminals decreased, resulting in high external force resistance and low internal friction loss, respectively. A2 exhibits the highest tear strength because the good filler dispersion and high degree of entanglement in A2 lengthen the propagation paths of tear cracks. However, the tear strength of A3 is not better than that of A2 because of the plasticizing effect of the dissociation reagent.

Dynamic Mechanical Properties

The storage modulus (E') vs. temperature (T) and tanδ vs. T curves of the three composites are shown in Figure 6, and the glass-transition temperatures are listed in Table VI.

As shown in Figure 6, the E' values of the three composites are similar in the glassy state, but there are two distinct differences in the high-elastic state. The order of E' for the three composites is A1 > A2 > A3, which is the same as that of Shore A

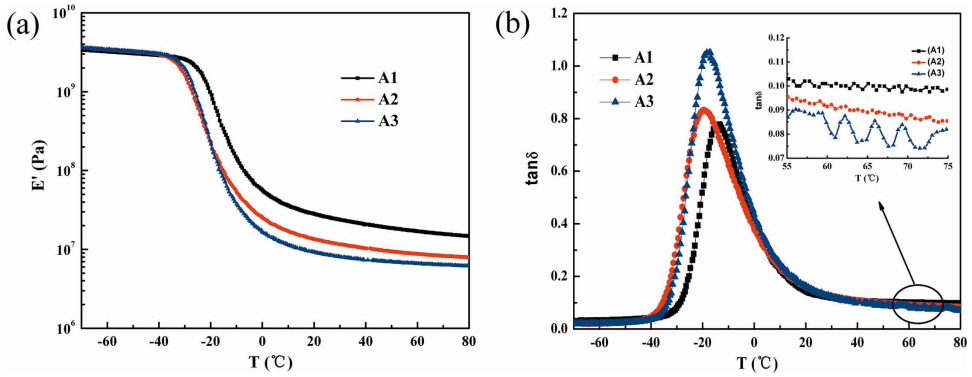

Figure 6. E' vs. T and tanδ vs. T curves of SiO_2–CB/S-SSBR and SiO_2–CB/ES-SSBR composites. [Color figure can be viewed in the online issue, which is available at wileyonlinelibrary.com.]

Table VI. T_g and tan δ of Three Kinds of Composites

Sample no.	A1	A2	A3
T_g (°C)	−13.5	−19.5	−17.9
tanδ at 0°C	0.404	0.381	0.431
tanδ at 60°C	0.101	0.092	0.085

hardness. At low strains (≤0.1%), E' of the vulcanizate in the high-elastic state can be used as an index to evaluate filler–filler interaction. A high E' indicates that there are many filler aggregates[11] induced by the strong filler–filler interaction[12] at the same formulation. As summarized in Table VI, the glass-transition temperatures of the three samples are different from one another, and $T_{gA1} > T_{gA3} > T_{gA2}$. The high glass-transition temperatures of A1 and A3 are related to their high vinyl contents. Compared with A1, the values of the tanδ half peak width of A2 and A3 both increase in the region of glass transition. The fact is that the macromolecular chains bound to the surface of filler is the most significant for A2 and A3, which leads to complication of motion unit during the defreezing process.

It is well known in the tire industry[13,14] that the value of tanδ at 0°C represents the wet-skid resistance, whereas the value of the tanδ at 60°C represents the rolling resistance of tread rubber. Therefore, high hysteresis at 0°C and low tanδ at 60°C will be favorable for wet-skid resistance and rolling resistance.[15] Table VI summarizes that the three composites have high tanδ at 0°C and low tanδ at 60°C, indicating that the contribution of reducing free-end and enhancing filler–matrix interaction to internal friction can be observed even at low strain conditions. As summarized in Table VI, A3 exhibits the highest tanδ at 0°C and the lowest tanδ at 60°C, achieving the balance of high wet-skid resistance and low rolling resistance.

The storage modulus (G') vs. ε and tanδ vs. ε curves of the three composites are shown in Figure 7.

As shown in Figure 7, the decreasing amplitude ($\Delta G'$) of G' with increasing strain (ε) is in the order A1 > A2 > A3. This order indicates that the Payne effect of A1 is the highest, that of A3 is the lowest, and that of A2 is close to that of A3, which illustrates that SiO_2 and CB disperse better in ES-SSBR than in SSBR. The Payne effect[16–18] has been widely used to describe the status of three-dimensional filler network formation. The lower the Payne effect the stronger the filler–polymer interaction and the better the filler dispersion.[19]

As shown in Figure 6, the tanδ values of all three composites exhibit the same trend with increasing strain. Furthermore, the tanδ values of A2 and A3 are far lower than that of A1 at the same strain. A3 has the lowest tanδ, indicating that the internal friction loss of end-functionalized samples decreases more significantly than unmodified samples in the shear mode at large deformations.

Microstructure of Composites

The TEM images of SSBR and ES-SSBR filled with CB and SiO_2 are shown in Figure 8.

As shown in Figure 8, the size of the spherical nanofiller in A2 and A3 is about 50 nm, and the filler is dispersed in the matrix homogeneously. Moreover, A3 shows better filler dispersity than A2, whereas the filler in A1 shows a bead-chain network structure and agglomeration phenomenon. Thus, it can be seen that the results observed in TEM are identical with the results forecast by dynamic mechanical properties for A2, A3 to have good filler dispersion.

The high-resolution transmission electron microscopy images and EDS spectra of SiO_2–CB/S-SSBR and SiO_2–CB/ES-SSBR-2 composites are shown in Figure 9.

In the images shown in Figure 9, according to X-ray energy spectra analysis, the light part looking like air bubbles is CB and the dark part is silica. Figure 8(b) shows that aggregates of three to five SiO_2 particles about 20 nm in diameter are inlaid into the CB networks, and the two kinds of nanofiller in the ES-SSBR-2 matrix exhibit outstanding doping dispersion. On the other hand, Figure 8(a) shows that the silica aggregates in the S-SSBR matrix are much bigger, and the dispersion of the two kinds of filler is worse than that in ES-SSBR-2. The EDS spectra analysis of A3 shows that the Si element is detected in the CB aggregates, whereas there is only a trace amount of Si in the CB aggregates in A1. The result further reveals that filler dispersion on a nanoscale can be effectively achieved by condensation reaction between the alkoxysilane groups at the ends of macromolecular chains and SiO_2 powder.

CONCLUSIONS

1. A S-SSBR and two end-functionalized S-SSBRs (ES-SSBR-1 and ES-SSBR-2) (coupling degree, 100%) with

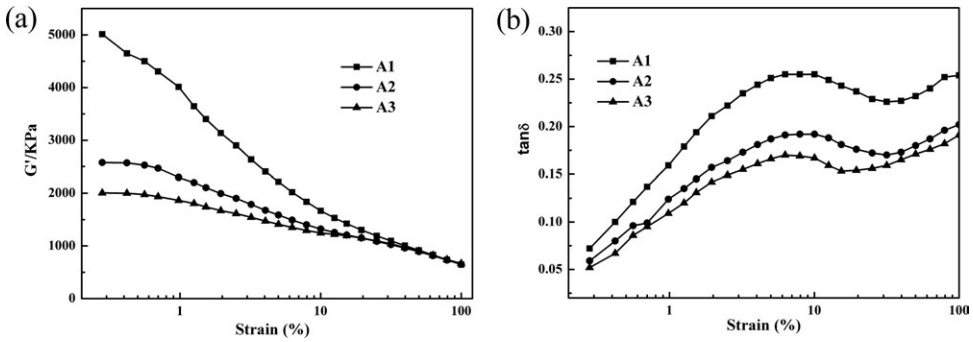

Figure 7. G' vs. ε and tanδ vs. ε curves of SiO_2–CB/S-SSBR and SiO_2–CB/ES-SSBR composites.

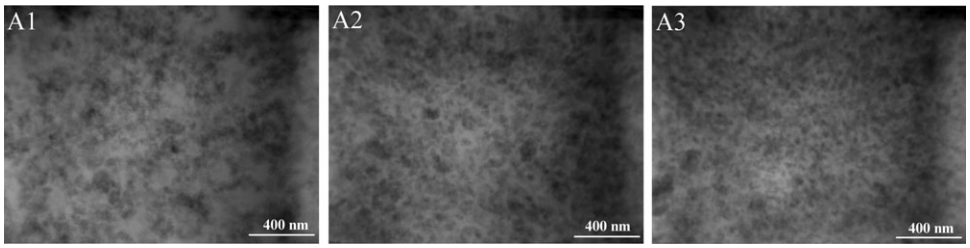

Figure 8. TEM images of SiO_2–CB/S-SSBR and SiO_2–CB/ES-SSBR composite vulcanizates.

alkoxysilane groups at the ends of molecular chains were synthesized by living anionic polymerization using a self-made multifunctional organic lithium initiator, and characterized by ^1H NMR. The calculated end-functionalized efficiencies of ES-SSBR-1 and ES-SSBR-2 reach 8.6 and 28.5%, respectively. The calculations were made using a method devised in our laboratory.

2. The mixing time of SiO_2 powder in ES-SSBR is 26% shorter than that in S-SSBR. The steady-state torque values of the two ES-SSBR/SiO_2 composites are 10 and 17% higher than that of the S-SSBR/SiO_2 composites, indicating that the strong affinity between SiO_2 powder and ES-SSBR results in good filler dispersion of SiO_2 powder in ES-SSBR.
3. The three composites are all shear-thinning, non-Newtonian fluids. The apparent viscosity of SiO_2–CB/ES-SSBR composites is slightly higher than that of SiO_2–CB/S-SSBR composites, indicating that it is the condensation reaction between the functional ends of molecular chains and the silica powder that contributes to the high viscosity and long relaxation during flow.
4. Compared with SiO_2–CB/S-SSBR composites, SiO_2–CB/ES-SSBR composites have better mechanical properties, higher wet-skid resistance, and lower rolling resistance. The two kinds of nanopowder in the ES-SSBRs exhibited outstanding doping dispersion and homogeneous distribution, indicating that after being coupled and end-functionalized, the two free ends of the macromolecular chains bonded chemically with the surface groups of CB and SiO_2 powder. Accordingly, ES-SSBR was a remarkable type of energy-saving elastomers.

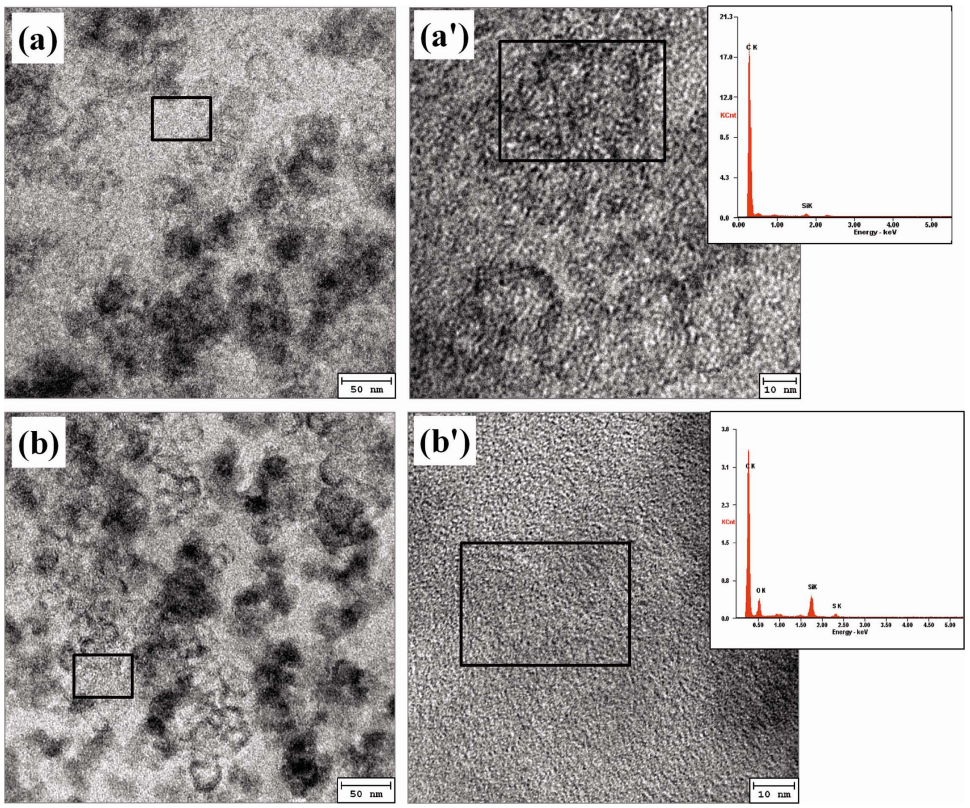

Figure 9. TEM images and EDS spectra of SiO_2–CB/S-SSBR and SiO_2–CB/ES-SSBR-2 composites: (a) (a′)—A1; (b) (b′)—A3. [Color figure can be viewed in the online issue, which is available at wileyonlinelibrary.com.]

ACKNOWLEDGMENTS

The authors gratefully acknowledge financial supports from the Tenth five-Year Plan of China (2004 BA 310 A 41) and the Natural Science Foundation of China (50573005).

REFERENCES

1. Pan, D. H.; Mei, Z. M. *Tyre Ind.* **2000**, *20*, 534.
2. Liu, L.; Zhang, L. Q.; Feng, Y. X.; Tian, M.; Wu, Y. P.; Jin, R. G. *China Rubber Ind.* **1999**, *4*, 245.
3. Zhao, S. H.; Zhang, J. M.; Zhang, X. Y.; Lu, J. M. *China Synth. Rubber Ind.* **2002**, *25*, 223.
4. Zhang, X. Y.; Jin, G. T.; Zhao, S. H. Can.Pat. 1, 148, 053, April 23, **1997**.
5. Zhang, X. Y.; Jin, G. T.; Zhao, S. H. Can.Pat. 1, 148, 050, April 23, **1997**.
6. JSR Bridgestone Co. Jpn. Pat. 01, 188, 501, July, **1989**.
7. Li, X. L.; He, M. L.; Zhang, X. Y.; Yao, M. *China Synth. Rubber Ind.* **2008**, *31*, 155.
8. Liu, X.; Zhao, S. H.; Zhang, X. Y.; Li, X. L.; Bai, Y. *China Rubber Ind.* **2009**, *56*, 325.
9. Wang, L.; Zhao, S. H.; Li, A.; Zhang, X. Y. *Polymer* **2010**, *51*, 2084.
10. Feng, H. D.; Zhang, X. Y.; Zhao, S. H. *J. Appl. Polym. Sci.* **2008**, *110*, 228.
11. Aso, O.; Eguiazábal, J. I.; Nazábal, J. *Comp. Sci. Technol.* **2007**, *67*, 2854.
12. Evans, L. R.; Fultz, W. C.; Huber, J. M. *Rubber World* **1998**, *219*, 38.
13. Zeng, Z. Q.; Yu, H. P.; Wang, Q. F.; Lu, G. *J. Appl. Polym. Sci.* **2008**, *109*, 1944.
14. Takino, H.; Nakayama, R.; Yamada, Y.; Kohjiya, S.; Matsuo, T. *Rubber Chem. Technol.* **1997**, *70*, 584.
15. Wang, M. J. *Rubber Chem. Technol.* **1998**, *71*, 520.
16. Payne, A. R.; Whittaker, R. E. *Rubber Chem. Technol.* **1971**, *44*, 440.
17. Payne, A. R. *J. Appl. Polym. Sci.* **1962**, *6*, 57.
18. Harwood, J. A. C.; Mullins, L.; Payne, A. R. *J. Appl. Polym. Sci.* **1965**, *9*, 3011.
19. Reuvekamp, L. A. E. M.; Ten Brinke J. W.; Van Swaaij, P. J.; Noordermeer, J. W. M. *Rubber Chem. Technol.* **2002**, *75*, 187.